

ARTICLE TYPE**Scaled ILU Smoothers for Navier-Stokes Pressure Projection**Stephen Thomas*¹ | Arielle K. Carr² | Paul Mullaney³ | Katarzyna Świrydowicz⁴ | Marcus S. Day⁵¹National Renewable Energy Laboratory, Golden, CO, USA, Email:

Stephen.Thomas@nrel.gov

²Department of Computer Science and Engineering, Lehigh University, Bethlehem, PA, USA, Email: arg318@lehigh.edu³AMD, Boulder, CO, USA, Email: Paul.Mullaney@amd.com⁴Pacific Northwest National Laboratory, Richland, WA, USA, Email: kasia.swirydowicz@gmail.com⁵National Renewable Energy Laboratory, Golden, CO, USA, Email: Marcus.Day@nrel.gov**Correspondence**

*Corresponding author

Summary

Incomplete LU (ILU) smoothers are effective in the algebraic multigrid (AMG) V -cycle for reducing high-frequency components of the error. However, the requisite direct triangular solves are comparatively slow on GPUs. Previous work has demonstrated the advantages of Jacobi iteration as an alternative to direct solution of these systems. Depending on the threshold and fill-level parameters chosen, the factors can be highly non-normal and Jacobi is unlikely to converge in a low number of iterations. We demonstrate that row scaling can reduce the departure from normality, allowing us to replace the inherently sequential solve with a rapidly converging Richardson iteration. There are several advantages beyond the lower compute time. Scaling is performed locally for a diagonal block of the global matrix because it is applied directly to the factor. Further, an ILUT Schur complement smoother maintains a constant GMRES iteration count as the number of MPI ranks increases, and thus parallel strong-scaling is improved. Our algorithms have been incorporated into hypre, and we demonstrate improved time to solution for linear systems arising in the Nalu-Wind and PeleLM pressure solvers. For large problem sizes, GMRES+AMG executes at least five times faster when using iterative triangular solves compared with direct solves on massively-parallel GPUs.

KEYWORDS:

iterative triangular solvers, GPU acceleration, ILU smoother, algebraic multigrid

1 | INTRODUCTION

We consider an incomplete LU (e.g., $ILU(k)$, $ILUTP$)¹ factorization used within the Algebraic Multigrid (AMG) method for the low Mach Navier-Stokes pressure solvers, PeleLM² and Nalu-Wind³. Analogous geometric multigrid methods (GMG) are employed in the NekRS^{4,5} and ExaDG⁶ pressure solvers. GMG operates on a hierarchy of nested grids with different resolutions and is effective for structured grid problems where the underlying mesh has a well-defined geometric structure. Our applications employ unstructured grids for which AMG is the appropriate choice. When employing ILU as smoothers within AMG, fast and accurate solvers for the resulting triangular systems are essential to achieve a low backward error. However, directly solving the triangular systems in the AMG solve phase may result in a significant performance bottleneck on massively parallel architectures. Iterative methods, like Richardson, offer an efficient alternative for approximating the sparse triangular solution^{7,8}, but these methods may fail to converge in a sufficiently small number of iterations when the L or U factor exhibit a high degree of non-normality. This can occur when factorizing ill-conditioned coefficient matrices⁹ and is the case with the two applications considered. When the triangular factors are close to normal, it becomes possible to use the significantly faster sparse matrix-vector (SpMV) products appearing in the Richardson iteration on GPU architectures. Thus, effective iterative methods avoid

a large departure from normality, $\text{dep}(U)$ or $\text{dep}(L)$, of the triangular factors. The large departure from normality and high condition number $\kappa(B)$ are mitigated by applying row scaling to the triangular factors. Substantial acceleration is thus achieved in the AMG solve phase for matrices of dimension larger than 10M exported from PeleLM² and Nalu-Wind³ compared with direct solves and iterative solves without scaling.

Linear systems of the form $Ax = b$, where A is a sparse symmetric $n \times n$ matrix, arise in “projection” methods for evolving variable-density incompressible and reacting flows in the low Mach flow regime. A is highly ill-conditioned when using cut-cell approaches to complex geometries, where non-covered cells that are cut by the domain boundary can have arbitrarily small volumes and areas². For instance, the matrices from the PeleLM combustion model in section 6.1 have singular values spanning sixteen orders of magnitude. Re-ordering the unknowns into blocks is one technique for handling non-normal factors⁸. However, a reordering algorithm such as the reverse Cuthill-McKee algorithm (RCM) can increase the computational cost.

Equilibration (i.e., scaling) techniques are generally designed to reduce the condition number of A ^{10, 11} and can therefore improve the accuracy of the solution to the linear system, particularly when using direct techniques¹. However, equilibration has received considerably less attention when used in conjunction with AMG. Even when equilibration is not performed, the L and U factors can be highly non-normal⁹. Indeed, equilibration of ill-conditioned A itself can also lead to highly non-normal factors L and U when subsequently computing the ILU factorization of A . In either case, when employing ILU smoothers that result in triangular factors with a large departure from normality, the use of Richardson iterative methods is rendered ineffective for approximately solving the triangular systems in the AMG solve phase. In these cases where we cannot reasonably avoid a high departure from normality a priori, and instead seek to reduce the departure from normality after the ILU factorization but prior to the triangular solve. We propose a technique to scale highly non-normal U factors using row scaling, $A \approx LDU$, where D is a diagonal matrix extracted from U by row scaling.² $\text{dep}(L)$ and $\kappa(L)$ remain modest, and thus we scale only the U factor. However, our approach extends to scaling both factors if necessary. Scaling leads to a significant reduction in both the condition number and departure from normality of the U factor¹³.

We also consider an ILUT Schur complement smoother and demonstrate that this maintains a constant Krylov solver iteration count as the number of MPI ranks increases. The Schur complement system represents the interface degrees of freedom at subdomain boundaries and are associated with the column indices corresponding to row indices owned by other MPI ranks in the hypre ParCSR block partitioning of the global matrix¹⁴. A single GMRES iteration is employed to solve the Schur complement system for the interface variables, followed by back-substitution for the internal variables using iterative triangular solves. A key observation is that the explicit residual computation $r^{(k)} = b - Ax^{(k)}$ is not needed for this single GMRES iteration, resulting in additional and significant computational cost saving. A hierarchical basis formulation of AMG based on the C-F block matrix partitioning and the Schur complement has been considered previously¹⁵, but can become expensive as the number of nonzeros in the coefficient matrix increases. A similar increase in cost is observed in our experiments, along with an increase in $\text{dep}(U)$ and $\|U_s\|_2$. In our approach, these are mitigated by limiting the fill-in and with row scaling and the Richardson iteration can again be effectively applied, resulting in the comparatively inexpensive solution of the triangular systems for the internal variables on the GPU. This paper is organized as follows. Section 2 presents the low Mach Navier-Stokes equations for the PeleLM and Nalu-Wind models. The AMG method is reviewed in section 3, along with smoothing techniques. Departure from normality and row scaling are also discussed. Equilibration of the triangular factors for the ILU smoother is presented in section 5. Implementation of AMG within the hypre¹⁴ solver library is described in section 6, where a performance model is provided, and results are presented for linear systems from the PeleLM² and Nalu-Wind¹⁶ pressure solvers. Conclusions are provided in section 7,

Contributions. To our knowledge, scaling of the L or U factors to reduce the condition number of the factors and thus mitigate high non-normality is a novel approach when applied within an ILU smoother for AMG. Incorporating our scaling strategy, along with the ILUT Schur complement smoother, into the AMG method applied to linear systems extracted from the PeleLM nodal pressure projection solver² and the Nalu-Wind pressure continuity solver³ facilitates a GMRES+AMG execution time of at least five times faster when using iterative triangular solves on massively parallel GPUs. Scaling, in particular, reduces the condition number of U and $\text{dep}(U)$ significantly, facilitating the use of a truncated Neumann series (Richardson) iteration to solve the triangular system. For the applications considered, scaling L was found to be unnecessary, but our approach can be easily extended to cases when scaling is needed for both triangular factors. Our algorithms were incorporated into hypre¹⁴. We demonstrate the effectiveness and efficiency of our approach for important problems arising in low Mach Navier-Stokes pressure solvers solved using AMG.

¹The instability of the solution to a linear system with an ill-conditioned coefficient matrix is well-known; see¹² Chapter 4.2

²Note that D can also be factored out from L .

2 | LOW MACH INCOMPRESSIBLE NAVIER-STOKES

2.1 | PeleLM Combustion Model

PeleLM is an adaptive mesh low Mach number combustion code developed and supported under DOE's Exascale Computing Project. PeleLM features a variable-density projection scheme to ensure that the velocity field used to advect the state satisfies an elliptic divergence constraint. Physically, this constraint enforces a consistently evolving flow with a spatially uniform thermodynamic pressure across the domain. A key feature of the model is that the discretization is based on a conservative embedded boundary approach to represent complex boundary shapes. Intersections of domain boundaries with the underlying Cartesian grid can lead to arbitrarily small cell faces and volumes, which in turn can lead to highly ill-conditioned matrices representing the elliptic projection operator.

The low Mach number flow equations represent the reacting Navier-Stokes flow equations in the low Mach number regime, where the characteristic fluid velocity is small compared to the sound speed, and the effect of acoustic wave propagation is unimportant to the overall dynamics of the system. Accordingly, acoustic wave propagation can be mathematically removed from the equations of motion, allowing for a numerical time step based on an advective CFL condition. This leads to an increase in the allowable time step of order $1/M$ over an explicit, fully compressible method, where M is the Mach number. In this mathematical framework, the total pressure is decomposed into the sum of a spatially constant (ambient) thermodynamic pressure and a perturbational pressure, $\pi(x, t)$, that drives the flow. The set of conservation equations specialized to the low Mach number regime is a system of partial differential equations with advection, diffusion, and reaction (ADR) processes that are constrained to evolve on the manifold of a spatially constant $P_0(t)$. Under suitable conditions, $\pi(x, t)/P_0(t) = \mathcal{O}(M^2)$.

$$\begin{aligned}\frac{\partial(\rho\mathbf{u})}{\partial t} + \nabla \cdot (\rho\mathbf{u} \otimes \mathbf{u} + \boldsymbol{\tau}) &= -\nabla\pi + \rho\mathbf{F}, \\ \frac{\partial(\rho Y_m)}{\partial t} + \nabla \cdot (\rho Y_m \mathbf{u} + \mathbf{F}_m) &= \rho\dot{\omega}_m, \\ \frac{\partial(\rho h)}{\partial t} + \nabla \cdot (\rho h \mathbf{u} + \mathbf{Q}) &= 0,\end{aligned}$$

ρ is the density, \mathbf{u} is the velocity, h is the mass-weighted enthalpy, T is temperature, Y_m is the mass fraction of species, and $\dot{\omega}_m$ is the molar production rate for species m . Additionally, $\boldsymbol{\tau}$ is the stress tensor, \mathbf{Q} is the heat flux and \mathbf{F}_m are the species diffusion fluxes. These transport fluxes require the evaluation of transport coefficients (e.g., the viscosity μ , the conductivity, and the diffusivity matrix D , all of which are computed using the library EGLIB¹⁷). The momentum source, \mathbf{F} , is an external forcing term. These evolution equations are supplemented by an equation of state for the thermodynamic pressure. For example, the ideal gas law,

$$P_0(\rho, Y_m, T) = \frac{\rho\mathcal{R}T}{W} = \rho\mathcal{R}T \sum_m \frac{Y_m}{W_m},$$

can be used, where W_m and W are the species and mean molecular weights, respectively. To close the system we also require a relationship between enthalpy, species, and temperature. We adopt the definition used in the CHEMKIN¹⁸ standard, and have $h = \sum_m Y_m h_m(T)$, where h_m is the species enthalpy. Note that expressions for $h_m(T)$ incorporate the heat of formation for each species. Neither species diffusion nor reaction redistribute the total mass, hence $\sum_m \mathbf{F}_m = 0$ and $\sum_m \dot{\omega}_m = 0$. Thus, summing the species equations and using the definition $\sum_m Y_m = 1$, we obtain the continuity equation:

$$\frac{\partial\rho}{\partial t} + \nabla \cdot \rho\mathbf{u} = 0$$

This, together with the conservation equations form a differential-algebraic equation (DAE) system that describes an evolution equation subject to the constraint of spatially constant thermodynamic pressure. A standard approach to attacking such a system computationally is to differentiate the constraint until it can be recast as an initial value problem. Following this procedure, set the thermodynamic pressure constant in the frame of the fluid, $DP_0/Dt = 0$ and observe that if the initial conditions satisfy the constraint, this expression will enforce that it continues to satisfy the constraint over all time. Expanding this expression via the chain rule and continuity:

$$\nabla \cdot \mathbf{u} = \frac{1}{T} \frac{DT}{Dt} + W \sum_m \frac{1}{W_m} \frac{DY_m}{Dt} = S.$$

Thus the constraint here takes the form of a condition on the divergence of the flow. Note that the actual expressions will depend upon the chosen models for evaluating the transport fluxes.

There are three different types of linear solves required to advance the velocity field. The first is the marker-and-cell (MAC) solve in order to obtain face-centered velocities used to compute advective fluxes. The second is the multi-component cell-centered solver that is used to obtain the provisional new-time velocities. Finally, a nodal solver is used to project these in order that they satisfy the constraint. We project the new-time velocity by solving the elliptic equation,

$$L \phi = D \left[\mathbf{u}^{n+1,*} + \frac{\delta t}{\rho^{n+1/2}} G \pi^{n-1/2} \right] - \hat{S}^{n+1} \quad (1)$$

for nodal values of ϕ and time index n . Here, L represents a Laplacian of nodal data, computed using the standard bilinear finite-element approximation to $\nabla (1/\rho^{n+1/2}) \nabla$. Also D is a discrete second-order operator that approximates the divergence at nodes from cell-centered data and G approximates a cell-centered gradient from nodal data. Nodal values for \hat{S}^{n+1} required for this equation are obtained by interpolating the cell-centered values. Finally, we determine the new-time cell-centered velocity field using

$$\mathbf{u}^{n+1} = \mathbf{u}^{n+1,*} - \frac{\delta t}{\rho^{n+1/2}} G (\phi - \pi^{n-1/2}) \quad (2)$$

2.2 | ExaWind Wind-Turbine Model

The ExaWind ECP project aims to simulate the atmospheric boundary layer air flow through an entire wind farm on next-generation exascale-class computers. The primary physics codes in the ExaWind simulation environment are Nalu-Wind and AMR-Wind. Nalu-Wind and AMR-Wind are finite-volume-based CFD codes for the incompressible-flow Navier-Stokes governing equations. Nalu-Wind is an unstructured-grid solver that resolves the complex geometry of wind turbine blades and thin blade boundary layers. AMR-Wind is a block-structured-grid solver with adaptive mesh refinement (AMR) capabilities that captures the background turbulent atmospheric flow and turbine wakes. Nalu-Wind and AMR-Wind models are coupled through overset meshes. The equations consist of the mass-continuity equation for pressure and Helmholtz-type equations for transport of momentum and other scalars (e.g. those for turbulence models). For Nalu-Wind, simulation times are dominated by linear-system setup and solution of the continuity and momentum equations. Both PeleLM and AMR-Wind are built on the AMReX software stack¹⁹, with hierarchical block structured meshes, and employ geometric multigrid as the primary solver, however, they both have the option of using the hypre library²⁰ to access alternative solvers, such as algebraic multigrid.

An implicit BDF time integrator was employed with an adaptive (variable) time-step that can increase towards a target Courant-Friedrichs-Lewy (CFL) number. The momentum and pressure solutions obtained during time stepping are calculated by an incremental approximate pressure projection algorithm. The momentum and pressure equations are segregated and solved sequentially with implicit advection/diffusion. To describe the approximate pressure projection algorithm, consider the block (indefinite, saddle-point) matrix form of the discrete equations

$$\begin{bmatrix} F & G \\ D & 0 \end{bmatrix} \begin{bmatrix} u \\ p \end{bmatrix} = \begin{bmatrix} f \\ 0 \end{bmatrix}, \quad (3)$$

where the matrix F will depend on the predicted, current and earlier time-levels. F contains discrete contributions to the momentum equations from the time derivative, diffusion, and linearized advection terms. $F = I/\Delta t + \mu L + N$, where L is the Laplacian and N linearized advection. The discrete gradient and divergence matrices are G and D respectively. The vector f contains the additional terms for the momentum equations, e.g., body force terms, lagged stress tensor terms, etc. The right-hand side contains the appropriate terms, e.g., for a non-solenoidal velocity field. For more details, see Thomas et al.³. In order to derive a projection scheme, consider the time-split system of equations,

$$\begin{bmatrix} F & G \\ D & 0 \end{bmatrix} \begin{bmatrix} u^{n+1} \\ \Delta p^{n+1} \end{bmatrix} + \begin{bmatrix} I & G \\ D & 0 \end{bmatrix} \begin{bmatrix} 0 \\ p^n \end{bmatrix} = \begin{bmatrix} f \\ 0 \end{bmatrix}, \quad (4)$$

where $\Delta p^{n+1} = p^{n+1} - p^n$. Consider the block factorization of the matrix

$$\begin{bmatrix} F & G \\ D & 0 \end{bmatrix} = \begin{bmatrix} F & 0 \\ D & -DF^{-1}G \end{bmatrix} \begin{bmatrix} I & F^{-1}G \\ 0 & I \end{bmatrix}. \quad (5)$$

Inversion of F to form the Schur complement matrix $M = -DF^{-1}G$ would be costly. The splittings approximate the inverse with the diagonal matrix $[\text{diag}(F)]^{-1}$. Nalu-Wind employs an approximate projection scheme that introduces an auxiliary projection time-scale, determined by the factor $B_2 = (\tau/\rho)I$. The factor $B_1 = -\tau L$ defines the linear system for pressure and approximates M . L is the Laplacian matrix obtained from the discrete form of the Gauss divergence theorem

These matrices are introduced into an approximate block factorization as follows

$$\begin{bmatrix} F & 0 \\ D & B_1 \end{bmatrix} \begin{bmatrix} I & B_2 G \\ 0 & I \end{bmatrix} \begin{bmatrix} u^{n+1} \\ \Delta p^{n+1} \end{bmatrix} + \begin{bmatrix} I & 0 \\ DB_2 & -B_1 \end{bmatrix} \begin{bmatrix} I & G \\ 0 & I \end{bmatrix} \begin{bmatrix} 0 \\ p^n \end{bmatrix} = \begin{bmatrix} f \\ 0 \end{bmatrix}.$$

The time scale $\tau = \Delta t$ is chosen for stabilization. The equations are solved for $\Delta \hat{u} = \hat{u} - u^n$, and Δp^{n+1} at each outer nonlinear iteration of the time step

$$F \Delta \hat{u} = f - G p^n - F u^n, \quad (6)$$

$$\tau L \Delta p^{n+1} = D (\rho \hat{u} + \tau G p^n) - \tau L p^n, \quad (7)$$

$$u^{n+1} = \hat{u} - \frac{\tau}{\rho} G \Delta p^{n+1}. \quad (8)$$

The momentum (6), and pressure-continuity (7) equations are solved separately within a fixed-point iteration for the incompressible system of equations. An iteration predicts a velocity field that is not necessarily divergence free and then projects that field to a divergence free sub-space. The matrix F and the right-hand side of the momentum equation are functions of the solution at time step $n + 1$ due to the choice of an implicit BDF time integrator. At each iteration, a better estimate for the solution is computed at time step $n + 1$ and hence a better estimate for F .

The pressure projection equations (1) and (7) are solved in discrete form with the GMRES+AMG iterative method described in the following sections. AMG is an optimal solver because the amount of computational work per degree of freedom in the resulting linear system remains constant as the problem size increases.

3 | ALGEBRAIC MULTIGRID

The AMG implementation to solve the linear system $Ax = b$ consists of two steps: the setup and solve phases. In the setup phase, the method constructs *prolongation* and *restriction* operators to transfer field data between coarse and fine grids. The application of these transfer operators leads to a sequence, or *hierarchy*, of successively lower dimension matrices, denoted $A_l \in \mathbb{C}^{m_l \times m_l}$, $l = 0, 1, \dots, m$ where $A_l = R_l A_{l-1} P_l$, $m_l < m_{l-1}$, and $m_0 = n$. In the Galerkin formulation of AMG, P_l is a rectangular matrix with dimensions $m_{l-1} \times m_l$ also referred to as the *interpolant* and $R_l = P_l^T$. Once the transfer operators are determined, the coarse-matrix representations are computed through sparse triple-product matrix-matrix multiplication.

In classical Ruge-Stüben AMG²¹, the *strength of connection threshold* determines whether points in the fine mesh are retained when creating a set of coarse points: The point j *strongly influences* the point i if and only if

$$|a_{ij}| \geq \theta \max_{k \neq i} |a_{ik}|,$$

where θ is the strength of connection threshold, $0 < \theta \leq 1$. The selected coarse points are retained at the next coarser level, and the remaining fine points are dropped. More information on the strong connection threshold to determine the set of coarse grid points as well as how to form the transfer operators are found in²¹. Let C_l and F_l be the coarse and fine points selected at level l , and let m_l be the number of grid points at level l . Then, $m_l = |C_l| + |F_l|$ and $m_{l+1} = |C_l|$. Here, the coarsening is performed row-wise by interpolating between coarse and fine levels and generally attempts to fulfill two contradictory criteria. In order to ensure that a chosen interpolation scheme is well-defined and of good quality, some close neighborhood of each fine point must contain a sufficient amount of coarse points to interpolate from. Hence, the set of coarse points must be rich enough but should also be sufficiently small in order to achieve a reasonable coarsening rate. Because the size of the linear systems decreases on each coarser level, the interpolation should lead to a sufficient reduction in the number of non-zeros at each level of the hierarchy compared with the number of non-zeros in the coefficient matrix for the original linear system.³

In the solve phase, the method employs the *V-cycle*, which is comprised of a relaxation (or smoothing) iteration coupled with a coarse grid correction.⁴ Beginning at the finest level, the method moves to the next coarser level by first performing a small number of *pre-smoothing* iterations to the solution of $A_l x_l = b_l$ at the l^{th} level of the *V-cycle*. It then computes the residual $r_l = b_l - A_l x_l$ and applies the restriction operator as $b_{l+1} = R_l r_l$ to move to the next coarser level. This process is repeated until the coarsest level is reached. The equations at the coarsest level are either solved using a direct solver, or using an iterative scheme if A_m is singular. Here, the method interpolates the coarse solution as a correction to the solution on the next finer level using prolongation, $x_l = x_l + P_k x_{l+1}$, followed by a small number of *post-smoothing* iterations. AMG methods are optimal for certain

³While the coarser matrices are technically more dense - as a ratio of non-zeros to the size of the matrix - these matrices have fewer rows and columns.

⁴The V-cycle is the simplest complete AMG cycle. Other processes may be used in place of the V-cycle, such as the W- or F-cycles²¹.

linear systems, (i.e., constant work per degree of freedom in A_0) through complementary error reductions by the smoother and solution corrections propagated from coarser levels. Consult Algorithm 1 for a description of the multigrid V -cycle.

Algorithm 1 Multigrid single-cycle (V -cycle) algorithm for solving $Ax = b$.

```

//Solve  $Ax = b$ 
Set  $x = 0$ 
Set  $v = 1$  for  $V$ -cycle
call Multilevel( $A, b, x, 0, v$ )

function MULTILEVEL( $A_l, b, x, l, v$ )
  // Solve  $A_l x = b$  ( $l$  is current grid level)
  // Pre smoothing step
   $x = S_l^1(A_l, b, x)$ 
  if ( $k \neq m$ ) then
     $r_{l+1} = R_l(b - A_l x)$ 
     $A_{l+1} = R_l A_l P_l$ 
     $v = 0$ 
    for  $i = 1 \dots v$  do
      MULTILEVEL( $A_{l+1}, r_{l+1}, v, l + 1, v$ )
    end for
     $x = x + P_l v$ 
    // Post smoothing step
     $x = S_l^2(A_l, b, x)$ 
  end if
end function

```

3.1 | Smoothing

Smoothers, or relaxation schemes, are generally implemented as an inexpensive iterative method such as Gauss-Seidel, Jacobi, or incomplete factorization, and rapidly reduce high-frequency components of the error by approximately solving the system of equations. Given an approximate solution, x_l , to the system $A_l x_l = b_l$ at the l^{th} level of the V -cycle, the general form of a residual smoothing technique can be expressed as $x_l^{(k+1)} = x_l^{(k)} + S r_l^{(k)}$, where $x_l^{(k+1)}$ is the updated solution after smoothing, S is the smoothing or damping factor, and $r_l^{(k)} = b_l - A_l x_l^{(k)}$ is the residual. When the remaining low-frequency error is restricted it then becomes higher frequency on the next, coarser level. A smoothing technique is employed until reaching the coarsest level of the V -cycle. Dropping the subscript l for ease of notation, the general form of a relaxation scheme for $Ax = b$ is given by

$$Mx^{(k+1)} = Nx^{(k)} + b \quad (9)$$

where $A = M - N$ is a *matrix splitting*, and $x^{(l+1)}$ represents the approximate solution at step $l + 1$ of the iterative method, and $r^{(l)}$ is the residual at the l^{th} step. For instance, the Gauss-Seidel iteration is based upon the splitting $M = D + L$, and $N = -U$, where L is the strictly lower and U the upper triangular part of the matrix A . The inverse of the matrix M is not formed, but rather direct triangular solvers are typically employed. However, as is the focus of this paper, these are relatively slow on GPU architectures. Adopting the notation used in⁷, the Jacobi iteration, is often written in the compact form

$$x^{(k+1)} = Gx^{(k)} + D^{-1}b, \quad (10)$$

with the regular splitting $A = M - N$, $M = D$ and $N = D - A$, and $G = I - D^{-1}A$.⁵

⁵Note that here we are referring to Jacobi in the context of AMG smoothers. Later, we will refer to it as an iterative solver for the L and U systems that result from employing the ILU smoother.

Polynomial smoothers rely on fast computation of the SpMV products. A polynomial type smoother¹⁶ is derived from the iterative solution of the triangular system for $(D + L)$ in Gauss-Seidel relaxation and then used to solve the linear system, $Ax = b$, where D is again the diagonal of A . An alternate formulation is to replace $(D + L)^{-1}$ with $(I + D^{-1}L)^{-1}D^{-1}$ in the preconditioned iteration, and replace the matrix inverse with a truncated Neumann series

$$x^{(k+1)} = x^{(k)} + \sum_{j=0}^p (-D^{-1}L)^j D^{-1} r^{(k)},$$

for $p < n$.

An ILU smoother is well-suited to handle highly varying matrix coefficients or anisotropic problems and is a generalization of Gauss-Seidel, where the diagonal matrix D represents row scaling of one (or both) of the triangular factors and $M = LDU$. Then we can write (9) as

$$x^{(k+1)} = x^{(k)} + M^{-1} (b - Ax^{(k)}) \quad (11)$$

An ILU factorization is particularly useful for sparse matrices, maintaining the sparsity pattern of the original matrix. It can be split into symbolic and numeric phases and if the sparsity pattern of the matrix A does not change on the finest level, then the symbolic phase of the factorization is often reused. For example, the sparsity pattern of the pressure matrix in the PeleLM model does not change during the fluid integration step, but could change between time steps as a result of a mesh refinement or regriding operation. This permits re-use of factorizations in the numeric phase in order to save computational time and avoid releasing and re-allocating storage for the L and U factors. This optimization opportunity exists only for the finest level in the multigrid hierarchy because the data-dependent coarsening algorithm may change the sparsity pattern on other levels.

An ILUT Schur complement smoother is also considered in¹ as part of a hierarchical basis formulation of AMG. Following Saad¹, Xu²² and Falgout et al.²³, a Schur complement preconditioner can be derived for the partitioned linear system

$$A \begin{bmatrix} x \\ y \end{bmatrix} = \begin{bmatrix} f \\ g \end{bmatrix}.$$

Consider the block $A = LU$ factorization of the coefficient matrix A

$$A = \begin{bmatrix} B & E \\ F & C \end{bmatrix} = \begin{bmatrix} I & 0 \\ FB^{-1} & I \end{bmatrix} \begin{bmatrix} B & E \\ 0 & S \end{bmatrix}.$$

The block matrix B is associated with the diagonal block (sub-domain) of the global matrix distributed across MPI ranks. The Schur complement is $S = C - FB^{-1}E$, and the reduced system for the interface variables, y , is given by

$$S y = g - F B^{-1} f \quad (12)$$

Then the internal, or local, variables represented by x are obtained by back-substitution according to the expression

$$x = B^{-1} (f - E y)$$

An ILUT Schur complement smoother for one level of the V -cycle in hypre is implemented as a single iteration of a GMRES solver for the global interface system (12). The local systems involving B^{-1} are then solved by computing an ILUT factorization of the matrix $B \approx LDU$.

We stress that the smoother employed on each level of the V -cycle does not have to be of the same type. Considering the aforementioned optimization of the ILU smoother on the finest level, this provides motivation for a mixed V -cycle with ILU smoothing only on the finest level for computational efficiency. However, even in the case of a mixed technique, when employing ILU smoothers on any level or all of them, care must be taken to ensure efficient solution of the resulting triangular systems. In Section 4 we provide background on bottlenecks imposed by ill-conditioning and non-normality in ILU factorizations when performing iterative triangular solves, and in Section 5 we propose our equilibration technique for mitigating these problematic characteristics, facilitating the use of fast iterative methods for solving the resulting triangular systems on GPUs.

4 | ITERATIVE TRIANGULAR SOLVES

A sparse triangular solver is a critical kernel in many scientific computing simulations, and significant efforts have been devoted to improving the performance of a general-purpose sparse triangular solver for GPUs²⁴. For example, the traditional parallel algorithm is based upon level-set scheduling, derived from the sparsity structure of the triangular matrix. Independent computations proceed within each level of the elimination tree. Overall, the sparsity pattern of the matrix can result in an extremely

deep and narrow tree, thereby limiting the amount of available parallelism for the solver to fully utilize many-core architectures, especially when compared to an SpMV sparse matrix-vector product. Multi-color reordering has been proposed as an alternative, however, this approach can adversely impact the convergence rate of the solver. In other words, there is little (or no) parallel work at most levels of the tree, and thus level scheduling does not provide significant speed-up, if any at all. Adopting an iterative approach leverages the speed of sparse matrix-vector products on GPUs. However, to facilitate fast convergence of the iterative triangular solves, we must address the concern of non-normality naturally introduced by the ILU factorization and exacerbated by poor choices in parameters.

4.1 | Convergence and Non-Normality

A *normal matrix* $A \in \mathbb{C}^{n \times n}$ satisfies $A^*A = AA^*$, and this property is referred to as *normality* throughout this paper. Intuitively, a *non-normal* matrix can be defined in terms of the difference between A^*A and AA^* . In the current paper, Henrici's definition of the *departure from normality* of a matrix is employed

$$\text{dep}(A) = \sqrt{\|A\|_F^2 - \|\Lambda\|_F^2}, \quad (13)$$

where $\Lambda \in \mathbb{C}^{n \times n}$ is the diagonal matrix containing the eigenvalues of A ¹³. Further information on metrics and bounds describing normality of matrices is found in^{13, 25, 26} and references therein.

In general, $\text{dep}(L)$ remains modest for the applications we consider in this paper, and the ILU factorization computes L such that $L = I + L_s$. Thus, scaling is not applied to L for these applications. Again, we note that our methods easily extend to those applications that require scaling of both triangular factors. However, the same observations are not true for $\text{dep}(U)$. In particular, scaling is necessary to produce $U = I + U_s$, with unit diagonal, where U_s is strictly upper triangular. Going forward, we will focus our discussion and notation on U .

It follows directly from the definition of normality that an upper (or lower) triangular matrix cannot be normal unless it is a diagonal matrix (see¹ Lemma 1.13 for a proof). Therefore, some departure from normality is expected in the L and U . However, if the departure from normality is too great, the iterations may diverge^{7, 27}. When the number of non-zeros in the factors is limited by larger drop tolerance and smaller fill-in levels in the incomplete factorization process, the number of non-zeros in U_s will decrease, and thus $\|U_s\|_F$ will become smaller. At the extreme, when fill-in is not allowed beyond the diagonal, then $U_s = 0$, and

$$\text{dep}(U) = \sqrt{\|I + U_s\|_F^2 - n} = \sqrt{\|I\|_F^2 - n} = 0. \quad (14)$$

Thus, dramatically restricting the number of non-zeros in the factors is one approach for bounding $\text{dep}(U)$ a priori. However, imposing constraints that result in factors that are too sparse generally produces an ILU factorization that is also too inaccurate (e.g., $\|A - LU\|_F = \gamma \gg 0$) to be useful. In other words, if LU is a poor approximation to A , we cannot reasonably expect an iterative solver to converge in few enough iterations to justify its use as a smoother. More generally, tuning the ILU parameters results in conservative or small $\text{nnz}(U)$ (and thus conservative $\text{nnz}(U_s)$), $\text{dep}(U)$ cannot grow too large.

4.2 | Effects of ILU Parameter Choice on (Non-)Normality

While the existing literature on the choice of parameters for ILU smoothers is limited, the work in⁹ provides a framework for studying the effect of parameter choices. Here, the relationship between these choices and the resulting sizes of $\text{dep}(U)$ is briefly examined, and subsequently the number of Jacobi iterations required. For a more in depth analysis of parameter choices, we refer the reader to^{9, 28}. The potential inaccuracy when the L and U have high condition numbers is first examined. When employing a threshold parameter (or drop tolerance) to limit the number of non-zeros in a row (or column) of the factors, the factorization of a symmetric matrix could be highly nonsymmetric⁹. One observable indicator is the vertical striping in the sparsity pattern of $L + U$, which signifies orders of magnitude difference in the entries of a row (or column) of the coefficient matrix A and is associated with ill-conditioning⁹.

Figure 1 displays the sparsity pattern of $L + U$ on the first four levels of AMG using the AMGToolbox²⁹ for matrix dimension $N = 14186$. Here, the drop tolerance is set to $1.e-15$ and fill limit to 200 per row using the ILUTP implementation in³⁰ with pivoting turned off.⁶ A very small drop tolerance and large fill-in are unreasonable choices for an ILU factorization because

⁶The term *pivoting* refers to row or column exchanges employed when a small *pivot*, or divisor, is encountered in the factorization. With pivoting turned off, the pivot is always the diagonal element.

they can substantially increase the cost associated with computing, applying and, storing the factors. The plots emphasize the resulting vertical striping associated with poorly chosen parameters, which is attributed to small pivots combined with large amounts of fill-in. The solution is to enforce a smaller fill level per row⁹. For a very ill-conditioned A , limiting the fill level per row may be insufficient to prevent ill-conditioned L and U . However, enforcing a fill level that is too conservative may result in a poor approximation of A . Figure 2 displays the non-zero pattern of $L + U$ for the same matrices as in Figure 1, but with the fill level per row now set to 10. The dramatic striping pattern is no longer present, however some remains, indicating the potential for ill-conditioning despite restricting the amount of fill.

An example demonstrating the effects of a conservative drop tolerance on the conditioning of A is omitted here, however, by imposing a very small drop tolerance, the resulting triangular solves may be unstable. This is due to the fact that the off-diagonal elements are much larger than those along the diagonal⁹. In fact, the prescription given in⁹ is to consider scaling to reduce $\kappa(A)$ with the warning that non-normal triangular factors may result. In Section 5.2, we demonstrate the effects of varying drop tolerances, combined with scaling of a judicious choice in drop tolerance followed by row/column scaling of factors results in very few iterations required to accurately solve the triangular systems.

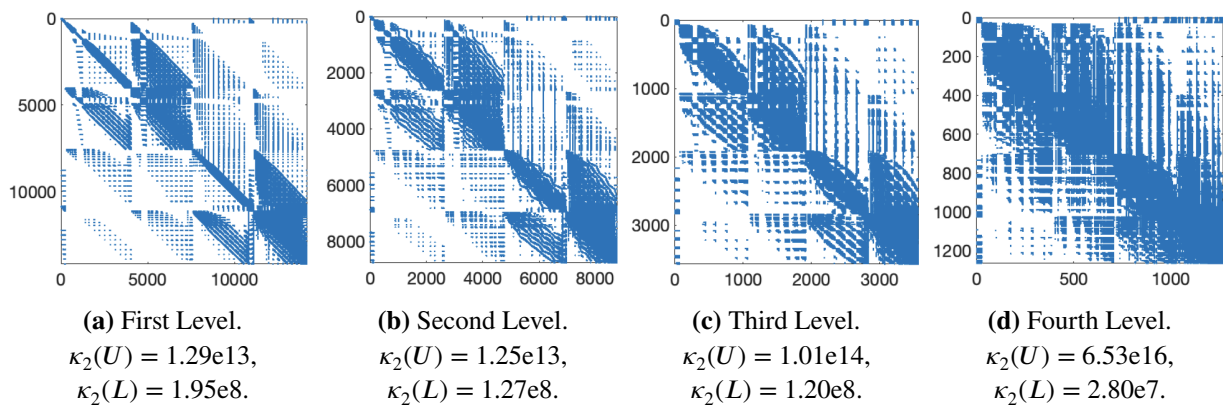


FIGURE 1 Non-zero patterns of $L + U$ for matrix size $N = 14186$ for the first four levels using AMGToolbox. Drop tolerance is set to $1.\text{e}-15$ and fill limit per row set to 200.

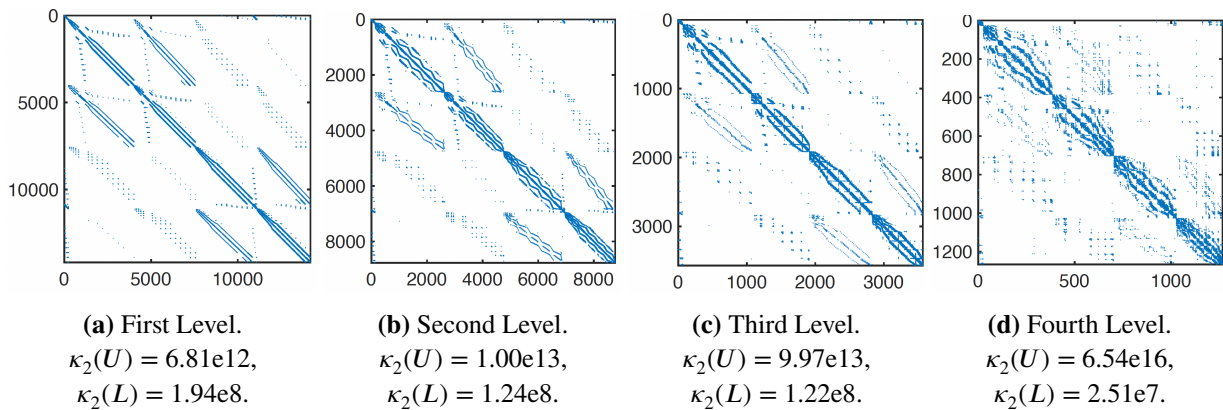


FIGURE 2 Non-zero patterns of $L + U$ for matrix size $N = 14186$ for the first four levels using AMGToolbox. PeleLM model. Drop tolerance is set to $1.\text{e}-15$ and fill limit per row set to 10.

5 | AN ILU SMOOTHER WITH SCALED FACTORS

To mitigate the high degree of non-normality of U , we propose row and column scaling, as well as row scaling alone, of the triangular factors within the smoothing step of AMG. We note again that in the applications considered, the L factor generally did not display ill-conditioning or high degrees of non-normality, and so we focus our discussion on U . By scaling U , and subsequently reducing both $\kappa(U)$ and $\text{dep}(U)$, we facilitate the use of the significantly faster SpMV products appearing in the Richardson iteration on GPU architectures to solve the triangular linear systems. We first introduce the general form of the scaled linear system and demonstrate the effects on $\kappa(U)$ and $\text{dep}(U)$ for several applications; see Section 5.1. Then, we expand the Richardson iteration explicitly to derive the Neumann series, demonstrating how the series can be truncated to very few terms; see Section 5.2.

5.1 | Equilibration to Reduce Non-Normality

Row and column scaling is a common choice for reducing ill-conditioning, but also extends to non-normal matrices arising in the ILU factorization of a highly ill-conditioned matrix. In doing so, we can expect the weight of the off-diagonal elements to decrease, particularly in the case of diagonally dominant matrices. Diagonal matrices D_l and D_r typically employ row or column norms. Specifically, row and column scaling results in a linear system that has been equilibrated and now takes the form

$$L D_r U D_c x = b. \quad (15)$$

The Richardson iterations are applied to the upper triangular matrix $D_r U D_c$ (in addition to the lower triangular factor L). Because $D_r U D_c$ has a unit diagonal, the iterations can be expressed in terms of a Neumann series, which is discussed next, in Section 5.2. When an LDU or LDL^T factorization is available, the diagonal matrix D can represent row scaling for either the L or U matrix. For the applications considered, only the U matrix is scaled, and thus row scaling is employed. Given an incomplete LU factorization, D can be written as

$$D = \text{diag}(U), \quad (16)$$

and the scaled \tilde{U} is subsequently defined as

$$\tilde{U} = D^{-1}U \quad (17)$$

to obtain the incomplete $LD\tilde{U}$ factorization from the incomplete LU factorization.

In Tables 1 and 2, the departure from normality and condition number of the factors, respectively, are given. We also compare $\kappa(U)$ and $\text{dep}(U)$ before and after scaling for matrices obtained from the SuiteSparse Matrix Collection³¹ (first five rows). Results for three matrices exported from PeleLM (final three rows) are also provided. Note that $\text{dep}(L)$ is generally very modest, and never as large as $\text{dep}(U)$. To generate these results Matlab's `ilu` was applied with setup type 'nofill' (i.e. ILU(0)).

Matrix	Dimension	$\text{dep}(L)$	$\text{dep}(U)$	$\text{dep}(D^{-1}U)$ (row scaling)	$\text{dep}(D_r U D_c)$ (row/col scaling)
af_0_0_k101	503625	326.95	1.84e8	326.95	320.89
af_shell1	504855	386.66	1.52e8	386.66	407.35
bundle_adj	513351	8.52e6	4.52e11	8.52e6	438.70
F1	343791	335.52	4.89e8	335.52	331.79
offshore	259789	231.86	7.05e15	231.86	222.71
PeleLM331	331	8.37	1.50e6	8.37	4.13
PeleLM2110	2110	16.99	1.09e7	16.99	9.33
PeleLM14186	14186	1.45e4	1.00e6	1.45e4	26.33

TABLE 1 Departure from normality for the L and U factors when applying an ILU(0) factorization to several matrices, followed by the departure from normality after row scaling and row/col scaling are applied to the U factor. The first five come from³¹, and the last three are extracted from PeleLM. Matlab's `ilu` with type 'nofill' was computed for all matrices.

Our results demonstrate that the scaling strategies substantially reduce $\text{dep}(U)$, and that in many cases, the row/column scaling produces a larger reduction compared with row scaling alone. However, in some cases, row scaling results in a lower

Matrix	$\kappa(A)$	$\kappa(L)$	$\kappa(U)$	$\kappa(D^{-1}U)$ (row scaling)	$\kappa(D_r U D_c)$ (Ruiz scaling)
af_0_0_k101	3.60e8	156.54	1.02e3	75.78	108.83
af_shell11	1.72e10	49.99	231.94	116.42	171.30
bundle_adj	6.10e15	4.59e12	3.53e14	2.93e12	2.37e3
F1	3.26e7	6.51e3	1.34e5	2.67e4	1.54e4
offshore	2.32e13	96.79	7.56e10	148.35	156.99
PeleLM331	3.48e17	14.06	3.87e9	43.06	18.72
PeleLM2110	3.21e17	13.39	4.41e9	34.02	12.31
PeleLM14186	6.64e15	1.83e8	6.87e12	1.74e7	9.51

TABLE 2 Condition number for A , L , and U when applying an ILU(0) factorization to several matrices, followed by the condition numbers after row scaling and Ruiz scaling are applied to the U factor. The first five come from³¹, and the last three are extracted from PeleLM. Matlab's `ilu` function with type 'nofill' was computed for all matrices.

departure from normality. When row scaling results in a smaller $\text{dep}(U)$, both are nearly the same, or at least of the same order of magnitude. The ILU smoother with scaling is provided in Algorithm 2. To employ row scaling within Algorithm 2, formation of D_U , D is constructed as in (16) and updated \tilde{U} as in (17). Here, only the U factor is scaled. The ILU factorization is assumed to result in a lower triangular matrix with unit diagonal, e.g. $L = I + L_s$ ⁷, which also generates a finite Neumann sum. For the ILUT Schur complement smoother, we again mitigate high degrees of non-normality by limiting fill-in, and it is important to note the residual vector is not required for the Schur complement GMRES solver for a fixed number of iterations. The initial guess is set to $x^{(0)} = 0$ and $r^{(l)} = b$, without a convergence check with the residual $r^{(l)}$.

Algorithm 2 ILU+Richardson smoother for AMG with row scaling of U .

```

Given  $A \in \mathbb{C}^{n \times n}$ ,  $b \in \mathbb{C}^n$ 
Define droptol and fill
Compute  $A \approx LU$  with droptol and fill imposed
Define  $m_L$  and  $m_U$ , total number of iterations for solving  $L$  and  $U$ 
Define  $y = 0$ ,  $v = y$ 
//Richardson iteration to solve  $Ly = b$ 
for  $k = 1 : m_L$  do
   $y = b - L_s y$ 
end for
Scale  $U$  and  $y$  to obtain scaled  $\tilde{U}$  and  $\tilde{y}$ , and  $D_k$ 
Let  $D_U = \text{diag}(\tilde{U})$ 
Define  $D = D_U^{-1}$ 
//Richardson iteration to solve  $\tilde{U}v = \tilde{y}$ 
for  $k = 1 : m_U$  do
   $v = D \tilde{y} - \tilde{U}_s v$ 
end for
//Update and unpermute the solution
 $v = Dv$ 
 $x = P^{-1}v$ 

```

⁷This is a reasonable assumption as many factorizations produce such a matrix; e.g. consider the `ilu` function in Matlab.

5.2 | Neumann Series and the Richardson Iteration

Our technique for scaling the triangular factors not only reduces the departure from normality, but also results in a finite Neumann series. First consider the Jacobi iteration for solving the linear system $Ax = b$. Note that Jacobi has been discussed previously as a smoother, but it is a well known iterative solver for an arbitrary linear system (unrelated to AMG). Given the preconditioner $M = D$, the non-compact form of (10) is given by

$$x^{(k+1)} = x^{(k)} + D^{-1} (b - Ax^{(k)}) \quad (18)$$

where D is the diagonal part of A . For the triangular systems resulting from the ILU factorization $A \approx LDU$ (as opposed to the regular splitting $A = D + L + U$), the iteration matrices are denoted G_L and G_U for the lower and upper triangular factors, L and U , respectively. Let D_L and D_U be the diagonal parts of the L and U and let I denote the identity matrix. Assume L has a unit diagonal, then

$$G_L = D_L^{-1} (D_L - L) = I - L, \quad (19)$$

$$G_U = D_U^{-1} (D_U - U) = I - D_U^{-1} U. \quad (20)$$

We next consider the effect of iterating with a scaled ILU factorization (e.g., ILU scaled with row/column scaling as in (15), or the row-scaled LDU using (17)). The iteration matrix (20) simplifies to $G_U = U_s$, where U_s is a strictly upper triangular matrix.⁸ To solve $Ux = b$ let $b_s = D_U^{-1}b$, and $U = I + U_s$. Then replace (10) with a Richardson iteration

$$x^{(k+1)} = b_s + (I - U) x^{(k)} = b_s - U_s x^{(k)} \quad (21)$$

where the unit diagonal is removed. After expanding it follows that

$$\begin{aligned} x^{(k+1)} &= b_s - U_s b_s + U_s^2 b_s - \dots + (-1)^k U_s^k b_s \\ &= (I - U_s + U_s^2 - \dots + (-1)^k U_s^k) b_s \\ &= (I + U_s)^{-1} b_s. \end{aligned} \quad (22)$$

Then, the inverse of U is expressed as a Neumann series

$$U^{-1} = (I + U_s)^{-1} = I - U_s + U_s^2 - \dots = \sum_{i=0}^n (-1)^i U_s^i, \quad (23)$$

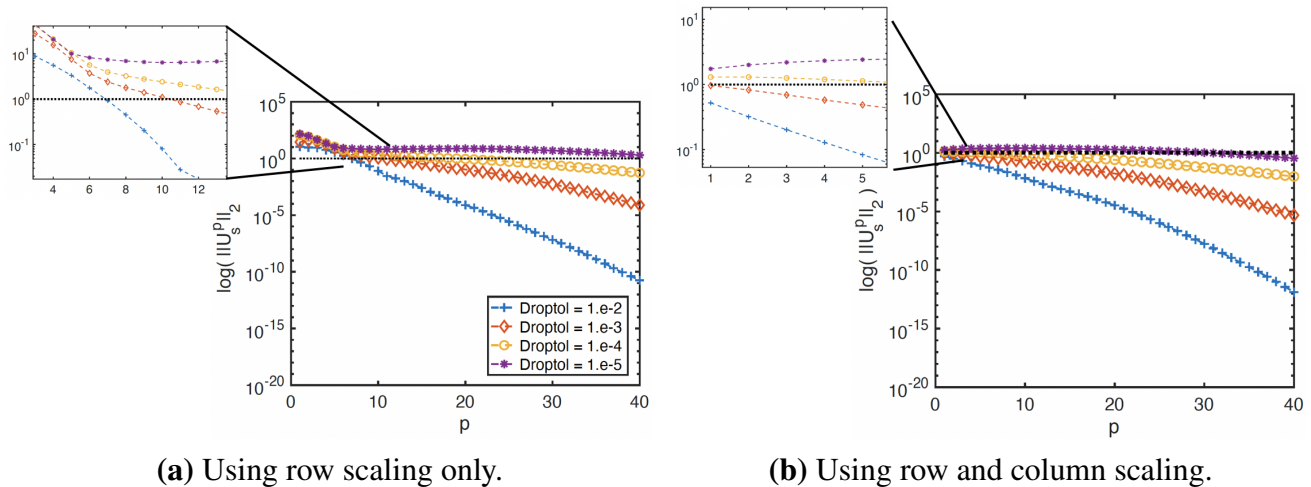
and with U_s strictly upper triangular and nilpotent, the above sum is necessarily finite.

The series in (23) converges when $\|U_s\|_2 < 1$, and in practice, this is true for the ILU(0) and ILUT for certain drop tolerances, where a convergent Neumann series is guaranteed. Even in cases when $\|U_s\|_2 \geq 1$, it is observed that $\|U_s^p\|_2 < 1$ for $p \ll n$, permitting truncation of the Neumann series - and thus the Richardson iteration - to a small number of terms. That $\|U_s^p\|_2$ eventually decreases is not unexpected because the number of possible non-zeros in U_s^p necessarily grows smaller as p grows larger when U_s is dense. However, numerical nilpotence is observed for $p \ll n$ in many cases for sparse U_s , and the size of p clearly depends on the number of non-zeros allowed in U and consequently U_s (either by imposition of small *droptol* or conservative fill, or both). In other words, $\|U_s^p\|_2$ is effectively zero much sooner than the theoretically guaranteed $\|U_s^n\|_2$.

Figure 3 displays $\|U_s^p\|_2$ when applying scaling to the ILU smoother employed at the finest level. Here, Matlab's `ilu` is used with type 'ilutp', threshold 0 (i.e. no pivoting), and various drop tolerances. For larger drop tolerances (i.e. *droptol* = $1.e - 2$ for both row/column and row scaling), $\|U_s^p\|_2 < 1$ for $p = 1$, giving convergence of the Neumann series. However, not for smaller drop tolerances. $\|U_s^p\|_2$ actually increases for the first few values of p , but eventually decreases and falls below 1. Figure 3a, displays $\|U_s^p\|_2$ for matrix dimension $N = 14186$ with row scaling. $\|U_s^p\|_2 < 1$ for modest p (e.g. $p = 7$ for *droptol* = $1.e - 2$). For smaller drop tolerances, p can be moderately large (e.g. $p = 45$ for *droptol* = $1.e - 2$).

The strategy is now extended to much larger linear systems exported from the Nalu-Wind¹⁶, and PeleLM² pressure solvers and a parallel performance analysis is provided. The Nalu-Wind matrix has dimension $N = 21M$ and is sufficiently large to exhibit differences in the strong scaling characteristics of the ILU Schur complement smoother. The PeleLM system of dimension $N = 11M$ is highly ill-conditioned and requires $\mathcal{O}(100)$ GMRES+AMG iterations to converge with a Gauss-Seidel smoother.

⁸Again, recall we omit discussion of L , and thus G_L for simplicity, as the applications demonstrate, do not exhibit problematic $\text{dep}(L)$.



(a) Using row scaling only.

(b) Using row and column scaling.

FIGURE 3 $\|U_s^p\|_2$ for $p = 1, 2, \dots, 40$, for $U = I + U_s$ using scaling and where U_s is the strictly upper triangular part of U . The black, dotted line represents the bound 1. PeleLM matrix dimension $N = 14186$.

6 | NUMERICAL RESULTS

Our iterative approach is applied to the solution of linear systems from the PeleLM² “nodal projection” step and the pressure continuity equation for the Nalu-Wind¹⁶ CFD model. Relatively large matrices of dimension, greater than 10M were exported from the PeleLM nodal pressure projection solver² and the Nalu-Wind pressure continuity solver¹⁶. Furthermore, scaling was applied directly to the non-normal U factor to reduce its departure from normality, facilitating the use of a Neumann series (Richardson iteration) to solve the triangular system. A performance model is also provided together with numerical and parallel scaling results in the following sections.

The stopping criteria for Krylov methods is an important consideration and is related to backward error for solving linear systems $Ax = b$. The most common convergence criterion found in existing iterative solver frameworks is based upon the relative residual, defined by

$$\frac{\|r_k\|_2}{\|b\|_2} = \frac{\|b - Ax_k\|_2}{\|b\|_2} < tol, \quad (24)$$

where r_k and x_k represent, respectively, the residual and approximate solution after k iterations of the iterative solver. An alternative metric commonly employed in direct solvers is the norm-wise relative backward error (NRBE)

$$NRBE = \frac{\|r_k\|_2}{\|b\|_2 + \|A\|_2 \|x_k\|_2}. \quad (25)$$

In numerical experiments, the norm-wise relative backward error for the solution of linear systems with GMRES was sometimes found to be lower than when the right-preconditioned GMRES was employed³². Indeed, the latter exhibited false convergence (the Arnoldi residual norm did not agree with the norm of the true residual $r^{(k)} = b - Ax^{(k)}$) when executed in parallel for highly ill-conditioned problems, $\kappa(A) > 10^{15}$. Flexible FGMRES¹ was found to be the most effective Krylov solver with an AMG preconditioner and did not exhibit false convergence.

The convergence of GMRES+AMG using ILU smoothers is compared with polynomial Gauss-Seidel. In particular, ILU on the finest level is combined with Gauss-Seidel on coarser levels. The choice to apply the ILU smoother on any number of levels – starting from the finest level – is now an option available in hypre²⁰. The ILU smoother on all levels and the ILUT Schur complement smoother are evaluated. The hypre-BoomerAMG library was designed for massively-parallel computation³³ and now also supports GPU acceleration of key solver components²³. The new formulation allows simple and efficient implementations that can utilize available optimized sparse kernels on GPUs¹⁶. Li et. al.³⁴ describe the class of M-M based interpolation operators suitable for efficient GPU computations.

6.1 | PeleLM Combustion Model

A sequence of three different size problems was examined, based on matrices exported from the PeleLM pressure continuity solver². The problem being solved is combustion in a piston-cylinder configuration, where the curved surface of the cylinder requires cut-cells through the mesh. The first of these matrices is a dimension $N = 14186$ linear system, solved with GMRES+AMG using the AMGToolBox^{29, 35} by applying ILUT smoothing only on the finest level $\ell = 1$, then ILUT on all levels and polynomial Gauss-Seidel smoothers. Iterative Richardson solvers are employed. Two pre- and post-smoothing sweeps were applied on all V -cycle levels, except for the coarse level direct solve. The AMG strength of connection threshold was set to $\theta = 0.25$. The convergence histories are plotted in Figure 4. The lowest iteration count results from using ILU(0) smoothing on all levels, however, the minimum compute time is obtained by using ILU(0) only on the finest level and polynomial Gauss-Seidel on the remaining levels. The iterative triangular solves fail to converge unless either a preconditioned Jacobi or Richardson iteration is employed. In the case of ILU(0), both row and row/column scaling exhibit similar convergence histories and thus row scaling is less costly in the set-up phase.

In the case of ILUT as the smoother, there are differences in the achievable GMRES error level between the row and row/column scaling, depending on the drop tolerances and level of fill per row. For the dimension $N = 14K$ problem, the norm-wise relative backward error (NRBE) is reported in Table 3 for $droptol = 1e-3$ and $lfill = 5$, where the NRBE is found to be an order of magnitude lower. A slightly lower backward error was obtained using two Richardson iterations with the row/column scaling versus three iterations using row scaling may not be sufficient to justify the additional set-up cost.

Richardson Iters.	5	4	3	2	1
Row scale U	5.85e-10	7.3e-10	5.94e-10	3.84e-10	5.35e-8
Row/col scale U	5.85e-10	7.17e-10	5.93e-10	3.85e-10	1.91e-9

TABLE 3 GMRES+AMG norm-wise relative backward error (NRBE) when using ILU+Richardson smoother with a varying number of Richardson iterations for the PeleLM matrices with dimension $N = 14186$, $droptol = 1e-3$, and $lfill = 5$. Row and Row/column scaling is applied to the U factor only.

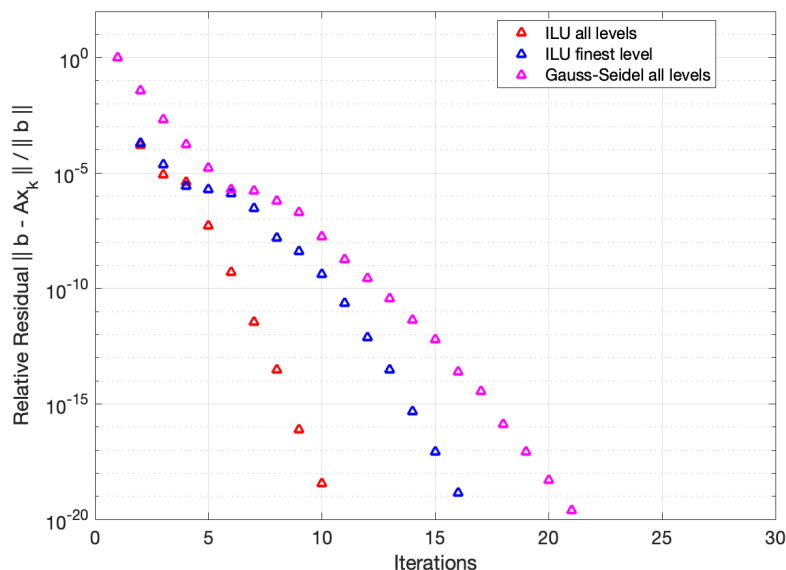


FIGURE 4 AMGToolBox results. PeleLM model. ILUT smoother on finest level versus all levels. Matrix size $N = 14186$.

Results using hypr-BoomerAMG for the $N = 1.4\text{M}$ linear system are plotted in Figure 5. These tests were performed on the NREL Eagle supercomputer with Intel Skylake CPUs and NVIDIA V100 GPUs. The parallel maximum independent set (PMIS) algorithm is applied together with aggressive coarsening and “MM-ext+i” interpolation are employed, with a strength of connection threshold, $\theta = 0.25$. Because the problem is very ill-conditioned, flexible FGMRES achieves the best convergence rates and the lowest NRBE. Iterative solvers were employed in these tests with ten (10) iterations. The convergence histories are plotted for mixed-ILUT, and polynomial Gauss-Seidel smoothers. The ILUT parameters were $droptol = 1e-2$ and $lfill = 10$. The lowest time for a single-GPU, was the ILUT smoother with Richardson iterations which achieved a solve time of 0.11 seconds.

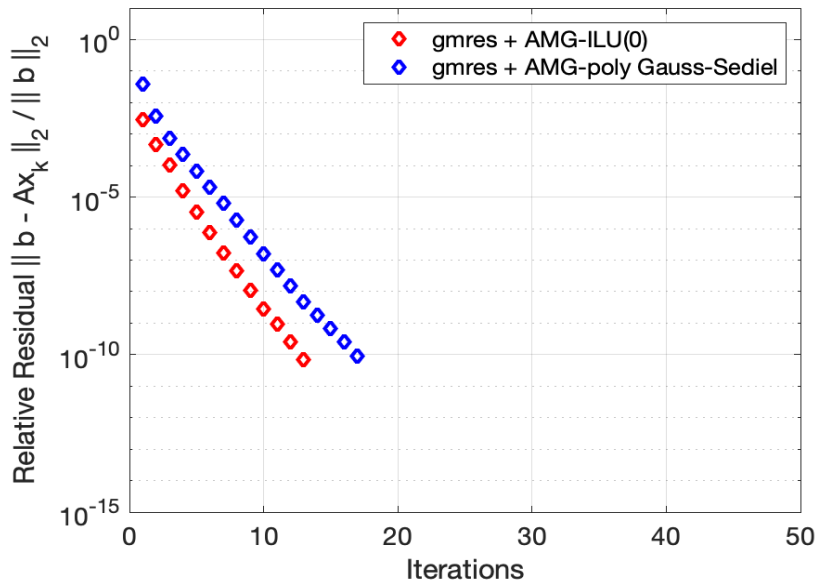


FIGURE 5 hypr-BoomerAMG GPU results NREL Eagle. Convergence history of (F)GMRES+AMG with polynomial, and mixed ILU smoothers with iterative solves. PeleLM model. Matrix size $N = 1.4\text{M}$

For comparison, a larger PeleLM linear system of dimension $N = 4\text{M}$ was run on the ORNL Crusher supercomputer (see Figure 6). The machine contains multiple compute nodes consisting of two AMD EPYC CPU sockets and four AMD MI250X GPU sockets, each containing two GCDs (GPU compute devices) for eight total. The same AMG parameters as the dimension 1.4M problem were specified, however, and ILU(0) smoother is applied on the first three V -cycle levels. The Richardson iterations are reduced to six (6) upper and five (5) lower per level. To reduce the relative residual to $1e-11$, the solve time is 0.11 seconds with iterative triangular solvers. Whereas, the solve time is 0.16 seconds when a direct solver is employed in the smoother. The speed-up is now reduced to $1.5\times$ on the AMD MI250X GPU and may be attributed to a faster implementation of the direct triangular solver by AMD. Despite the increased number of GMRES+AMG iterations for the polynomial Gauss-Seidel smoother, the solve time is 0.16 seconds, which is comparable to the direct solves with ILU. However, the number of GMRES iterations has grown from the smaller problem and is expected to increase further at larger problem sizes.

6.2 | Exa-Wind Fluid Mechanics Models

In Nalu-wind, the pressure systems are solved using MGS-GMRES with an AMG preconditioner, where a polynomial Gauss-Seidel smoother is described in Mullenney et al.¹⁶. Hence, Gauss-Seidel is a compute time intensive component, when employed as a smoother within an AMG V -cycle. The McAlister experiment for wind-turbine blades is an unsteady RANS simulation of a fixed-wing, with a NACA0015 cross section, operating in uniform inflow. Resolving the high-Reynolds number boundary layer over the wing surface requires resolutions of $\mathcal{O}(10^{-5})$ normal to the surface resulting in grid cell aspect ratios of $\mathcal{O}(40k)$. These high aspect ratios present a significant challenge. Overset meshes were employed to generate body-fitted meshes for the wing and the wind tunnel geometry. The simulations were performed for the wing at a 12 degree angle of attack, 1m chord length, denoted

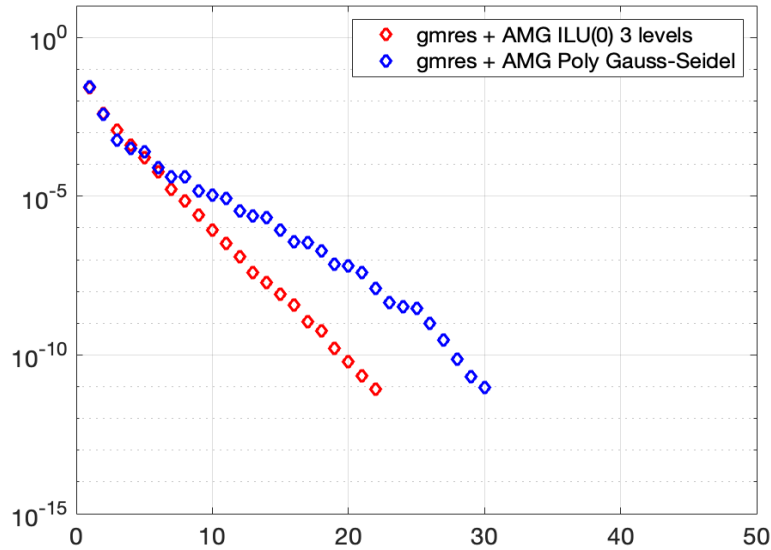


FIGURE 6 hypre-BoomerAMG GPU results NREL Eagle. Convergence history of (F)GMRES+AMG with polynomial, and mixed ILU smoothers with iterative solves. PeleLM model. Matrix size $N = 4M$

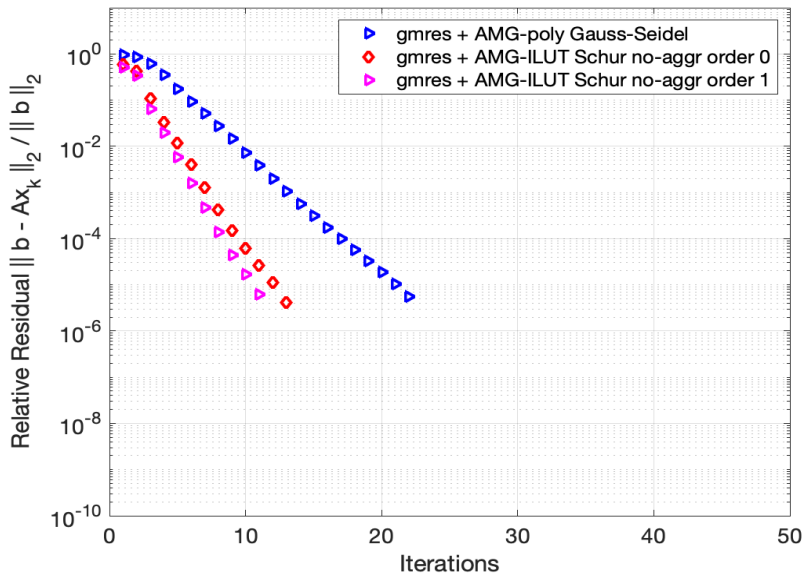


FIGURE 7 hypre-BoomerAMG GPU results an NREL Eagle. Nalu-Wind. Convergence history of (F)GMRES+AMG with polynomial, and ILUT Schur Complement smoothers with iterative solves. Matrix size $N = 23M$

c , 3.3 aspect ratio, i.e., $s = 3.3c$, and square wing tip. The inflow velocity is $u_\infty = 46$ m/s, the density is $\rho_\infty = 1.225$ kg/m³, and dynamic viscosity is $\mu = 3.756 \times 10^{-5}$ kg/(m s), leading to a Reynolds number, $Re = 1.5 \times 10^6$. Wall normal resolutions were chosen to adequately represent the boundary layers on both the wing and tunnel walls. The $k - \omega$ SST RANS turbulence model was employed for the simulations. Due to the complexity of mesh generation, only one mesh with approximately 3M grid points was generated.

Coarsening is based on the parallel maximal independent set (PMIS) algorithm allowing for a parallel setup phase. The strength of connection threshold is set to $\theta = 0.25$. Aggressive coarsening is applied on the first two V -cycle levels with multi-pass interpolation and a stencil width of two elements per row. The remaining levels employ M-M extended+i interpolation, with truncation level 0.25 together with a maximum stencil width of two matrix elements per row. The smoother is hybrid block-Jacobi with two sweeps of polynomial Gauss-Seidel applied locally on an MPI rank and then Jacobi smoothing for globally shared degrees of freedom. The coarsening rate for the wing simulation is roughly $4\times$ with eight levels in the V -cycle for hypre. Operator complexity C is close to 1.6 indicating more efficient V -cycles with aggressive coarsening, however, an increased number of GMRES iterations are required compared to standard coarsening. The comparison among ℓ_1 -Jacobi, Gauss-Seidel and the polynomial Gauss-Seidel smoothers is shown in Figure 8.

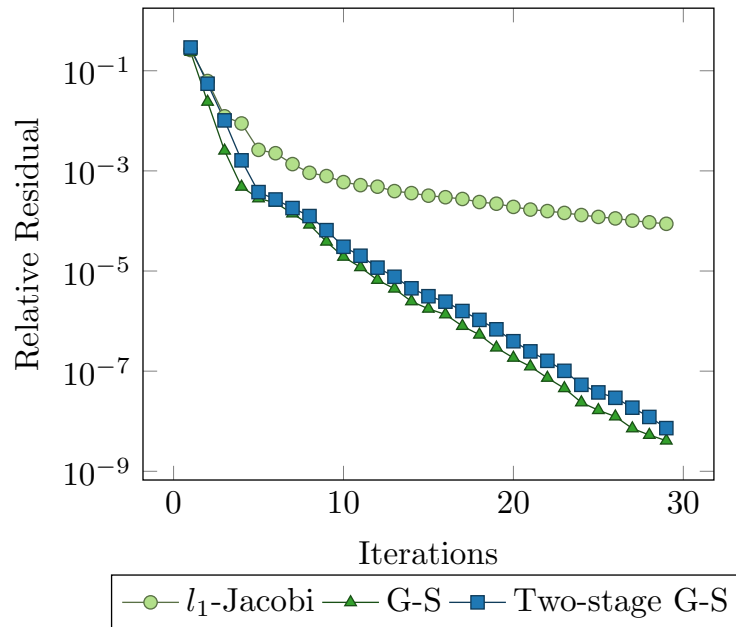


FIGURE 8 GMRES+AMG with ℓ_1 -Jacobi, Gauss-Seidel and polynomial Gauss-Seidel smoothers for a linear system from Nalu-Wind model with dimension $N = 3.1M$.

In order to evaluate the differences between the direct and iterative triangular solvers employed in the smoother, the compute times for a single GMRES+AMG pressure solve are given in Table 4. The ℓ_1 -Jacobi smoother from hypre is included for comparison. Both the CPU and GPU times are reported for the NREL Eagle supercomputer with Intel Skylake Xeon CPUs and NVIDIA V100 GPU's. In all cases, one sweep of Gauss-Seidel and two sweeps of ℓ_1 -Jacobi are employed because the number of sparse matrix-vector multiplies are equivalent in both cases. Either one CPU core or GPU was employed in these tests. The time reported corresponds to when the relative residual has been reduced below $1e-5$.

	ℓ_1 -Jacobi	Gauss-Seidel	Poly G-S
iterations	36	18	21
CPU (sec)	19.4	12	19.5
GPU (sec)	0.37	3.2	0.27

TABLE 4 GMRES+AMG compute time. Jacobi, Gauss-Seidel and Polynomial Gauss-Seidel Smoothers for a linear system from Nalu-Wind model with dimension $N = 3.1M$.

The timing results indicate the solver time with Gauss-Seidel is lower than when the ℓ_1 Jacobi smoother is employed on the CPU. However, the latter is more computationally efficient on the GPU. Whereas the polynomial Gauss-Seidel smoother leads

to the lowest compute times on the GPU and results in a 10X speed-up compared to the smoother that employs a direct triangular solver.

The NREL 5-MW turbine is a notional reference turbine with a 126 meter rotor that is appropriate for offshore wind studies. These models use inflow and outflow boundary conditions in the directions normal to the blade rotation and symmetry boundary conditions in other directions. For each simulation, 50 time steps are taken from a cold start with four Picard iterations per time step. Convergence histories for one such pressure linear system (after reaching steady-state) are displayed in Figure 7 for the ILUT-Schur complement and polynomial Gauss-Seidel smoothers. The former requires half as many iterations to reach the $1e-5$ convergence tolerance. Furthermore, a coarse-fine (C-F) ordering of the degrees of freedom results in fewer iterations. The strength of connection parameter was set to $\theta = 0.57$, which contributes to a reduction in the AMG set-up time. In addition, the ILU drop tolerance was $droptol = 1.0 \times 10^{-2}$, with a fill level per row of $l_{fill} = 2$. Sufficient smoothing was achieved with 18 iterations for the lower triangular L solve and 31 for the U solve. Aggressive coarsening was not specified and a single level of ILU smoothing was applied.

6.3 | V -Cycle GPU Performance Model

A mixed AMG algorithm is obtained with ILU smoothing on the finest levels of the AMG V -cycle hierarchy (e.g. level 1), followed by polynomial Gauss-Seidel or ℓ_1 -Jacobi on the remaining levels. In the numerical results reported earlier, the ILU smoothing is used on all levels and also in the mixed configuration for comparison. The latter requires fewer sparse matrix-vector multiplies and thus is more efficient.

The floating point operation count of the V -cycle, is determined by the number of non-zeros in the factors. The ILU smoother requires twenty (20) Richardson iterations and one outer sweep. These are applied during *pre-* and *post-smoothing* or twice. Therefore, the total number of flops required for the V -cycle with ILU(0) smoothing on every level is given by the sum below, where an SpMV costs $2 \times \text{nnz}(A_l)$ on level l ,

$$\text{flops} = \sum_{l=1}^{N_l-1} \text{nnz}(A_l) \times 80 \quad (26)$$

whereas the factor 80 is replaced by 8 for the polynomial smoother of degree two. This makes a compelling case for the mixed AMG approach with a combination of ILU and ℓ_1 -Jacobi smoothers when the convergence rate is improved and leads to lower flop counts. The cost of the coarse grid direct solve is $\mathcal{O}(N_c^3)$, where N_c is the dimension of the coarsest level matrix A_c , and is small in comparison. The cost of the Krylov iteration is dominated by the SpMV with the matrix A , whose cost is given by $2 \times \text{nnz}(A)$.

The compute time of a sparse direct triangular solver on a many-core GPU architecture such as from the NVIDIA cuSparse library is much higher than the SpMV. For the NVIDIA V100 GPU architecture, the SpMV can now achieve on the order of 50 – 100 GigaFlops/sec in double precision floating point arithmetic. When the number of GMRES+AMG iterations to achieve the same NRBE remains less than two times larger, then the case for employing the mixed scheme on GPUs becomes rather compelling.

Level	n_ℓ	$\text{nnz}(A)$
$\ell = 1$	11498575	306389891
$\ell = 2$	171074	6919886
$\ell = 3$	19658	1256596
$\ell = 4$	2018	126882
$\ell = 5$	232	10070
$\ell = 6$	29	605
$\ell = 7$	5	25

TABLE 5 Size and number of non-zeros for A , at each level, where n_ℓ denotes the matrix size at level ℓ . hypre-BoomerAMG. Aggressive coarsening. Matrix size $N = 11.49\text{M}$.

The compute time for the AMG V -cycle with GMRES SpMV is largely determined by the memory bandwidth (BW) between the GPU main memory and the thread processors. For the AMD MI250X GPU employed on Crusher and Frontier, the maximum achievable BW is 1.6 TeraBytes/sec. Our performance estimates are based on a roof-line model for the GPU and assumes we are in the bandwidth dominated regime. We also assume that computation and data movement are not overlapped. The transfer speed of sparse matrices (CSR format assumed) between the GPU memory and the thread processors is the dominant cost. More specifically, the P/R prolongation-restriction matrices, the coarse A_c , L and U factors, and the diagonal D are read at each level i of the V -cycle hierarchy with the row sizes and nnz given in Table 5. The transfer times are estimated in the model given below, where it is assumed that CSR matrix reads achieve $2/3$ of peak bandwidth.

$$\begin{aligned} \text{Ac_transfer} &= \text{nnz}(i) \times 8 \\ \text{L_U_transfer_Jacobi} &= \text{nnz}(i) \times 8 \\ \text{P_R_transfer} &= 2 \times \text{nnz}(i) \times 8 \\ \text{D_transfer_Jacobi} &= \text{rows}(i) \times 8 \\ \text{matrix_transfer_cost} &= \text{nnz}(1) \times 8 \\ \text{A_transfer} &= \text{matrix_transfer_cost} \\ \text{ILU}_{\text{Jacobi}}(i) &= \text{Ac_transfer} + \text{P_R_transfer} + \text{D_transfer_Jacobi} \end{aligned}$$

Assuming $N = 11 \times 10^6$ rows and 26 nnz per row, and a computation efficiency of 200 GigaFlops/sec:

$$\begin{aligned} \text{FLOPs time} &\approx \frac{6 \times 40 \times 26 \times N}{200 \times 10^9} = 0.35 \text{ sec} \\ \text{Memory transfer time} &= \frac{2 \times \text{sum}(\text{ILU}_{\text{Jacobi}}) + \text{A_transfer}}{1.6 \times 10^{12} \times 8 \times 40} = 3.05 \text{ sec} \\ \text{Total time} &= \text{FLOPs time} + \text{Memory transfer time} = 3.5 \text{ sec} \\ \text{Measured} &: 3.7 \text{ sec} \end{aligned}$$

In practice, the above model is remarkably accurate. For the matrix size $N = 11.49\text{M}$ and 40 GMRES+AMG iterations on a single GPU, we estimate a run time of 3.5 sec, and measured, 3.7 sec. In addition, the estimated ratio $\text{ILU}_{\text{GaussSeidel}}/\text{ILU}_{\text{Jacobi}} = 1.3$ is measured as 1.3. Therefore the V -cycle with ℓ_1 -Jacobi is 30% more efficient (faster) than when using Gauss-Seidel on the coarser levels to achieve the same relative residual error tolerance of $1e-6$.

The compute times of the GMRES+AMG solver in hypre with an incomplete LDU smoother, and either direct or iterative solvers in the ILU smoother, are compared below for the NVIDIA V100 GPU. The compute times for a single pressure solve are given in Table 6 for the $N = 14186$ dimension matrix. The ILU(0) and ILUT smoothers are included for comparison. Both the CPU and GPU times are reported. In all cases, two Gauss-Seidel and one ILU sweep are employed. The solver time reported again corresponds to when the relative residual decreases below $1e-5$.

	Gauss-Seidel	Poly G-S	ILUT direct	ILUT iter	ILU(0) iter
iterations	7	9	7	7	5
CPU (sec)	0.037	0.025	0.025	0.035	0.038
GPU (sec)	0.021	0.0067	0.032	0.0065	0.0048

TABLE 6 GMRES+AMG compute time on V100. Gauss-Seidel, polynomial Gauss-Seidel, and ILU smoothers. PeleLM matrix dimension $N = 14186$

Consider the CPU compute times for a single solve. The results indicate that the GMRES+AMG solver time using the mixed V -cycle with an ILU(0) smoother on the first level, versus a direct solver for the L and U systems, costs less than Gauss-Seidel smoothing on all levels. The PMIS algorithm is employed along with aggressive coarsening on the first V -cycle level. One sweep of the Gauss-Seidel smoother is employed in both configurations. The longer time is primarily due to the higher number of Krylov iterations required to converge. The ILUT smoother, on the finest level, with iterative solvers is the more efficient approach on the GPU. Despite only ten (10) SpMV products to solve the L and 15 to solve the U systems, the computational speed of the GPU for the SpMV kernel is more than sufficient to overcome the cost of a direct solve. The observed solver time

was 0.0065 with a performance model estimate of 0.0055 sec when $N = 14186$ and requires twenty iterations to converge where aggressive coarsening with hypre reduces the $\text{nnz}(A)$ per level³⁶.

The compute times for a larger dimension problem where $N = 1.4\text{M}$ are reported in Table 7. Here it was observed that the ILU(0) compute time on the GPU is lower than with the polynomial Gauss-Seidel smoother. Most notably, the GPU compute time for ILU(0) solves with fifteen (15) SpMV for U are two times faster than ILUT with direct solves. To further explore the parallel strong-scaling behaviour of the iterative and direct solvers within the ILU smoothers, the GMRES+AMG solver was employed to solve a PeleLM linear system of dimensions $N = 11\text{M}$. The LDU form of the factorization with row scaling was again employed and twenty (20) SpMV provide sufficient smoothing for this much larger problem. The linear system solver was tested on the NREL Eagle Supercomputer configured with two NVIDIA Volta V100 GPUs per node. Most notably, the solver with iterative Neumann scheme achieves a faster solve time compared to the direct solver as displayed in Figure 10. The convergence histories of the GMRES+AMG solver with a polynomial Gauss-Seidel and the ILU direct and iterative smoothers are plotted in Figure 9.

The larger problem was run on the ORNL Crusher supercomputer and the compute times on up to 128 MPI ranks are displayed in Figure 11. The combined solve and set-up times are plotted for direct and iterative triangular solvers. For a low number of MPI ranks, the direct triangular solver from AMD is more efficient than the iterative solves with SpMV. However, as the number of ranks increases, the iterative triangular solver for the smoother leads to lower compute times. The cross-over point for iterative solves occurs after thirty-two GPUs where the compute time continues to drop significantly faster. By comparing the times in Figures 10 and 11, it is observed that the AMD MI250X GPU is roughly four times faster than the NVIDIA V100 for this problem.

A strong-scaling study for the low resolution NREL 5 MegaWatt single-turbine mesh is displayed in Figure 12. The matrix dimension for this problem is $N = 23\text{M}$. The total setup plus solve time is displayed for (F)GMRES+AMG executing on the NREL Eagle supercomputer using two NVIDIA V100 GPUs per node on up to 20 nodes or 40 GPUs. The solve time is plotted for the polynomial Gauss-Seidel and ILUT Schur complement smoothers. In the latter case, a single iteration of the iterative GMRES solver, without residual computations, results in a steeper decrease in the execution time and improved performance. In addition, the number of GMRES+AMG solver iterations to reach a relative residual tolerance of $1e-5$ remains constant at eleven (11) as the number of compute nodes is increased.

	Gauss-Seidel	Poly G-S	ILUT direct	ILUT iter	ILU(0) iter
iterations	7	9	8	8	4
CPU (sec)	9.2	9.6	4.3	6.9	6.8
GPU (sec)	0.29	0.055	0.098	0.058	0.042

TABLE 7 GMRES+AMG compute time on V100. Gauss-Seidel, polynomial Gauss-Seidel, and ILU smoothers. PeleLM matrix dimension $N = 1.4\text{M}$.

7 | CONCLUSIONS

For the highly ill-conditioned PeleLM nodal pressure projection linear systems, the standard Jacobi and Gauss-Seidel smoothers are less effective for reducing the error at each level of the AMG V -cycle and may result in very large iteration counts or fail to converge for the preconditioned Krylov solver. Jomo et al.³⁷ compare PCG+AMG with Jacobi and Gauss-Seidel smoothers with GMRES preconditioned by ILU. However, they did not investigate ILU as a smoother for AMG. We proposed a novel approach for the solution of sparse triangular systems for the L and U factors of an ILU smoother for AMG. Previous work by H. Anzt, and E. Chow demonstrated that these factors are highly non-normal, even after appropriate re-ordering and scaling of the linear system $Ax = b$ and, Jacobi iterations may diverge. In order to mitigate the effects of a high degree of non-normality, as measured by Henrici's metric, either a row or row/column scaling is applied to the U factor during the set-up phase of the AMG V -cycle. A finite Neumann series multiplied by a vector is then computed, which is equivalent to a Richardson iteration. Our results demonstrate that several orders of magnitude reduction in the departure from normality $\text{dep}(U)$ is possible, thus leading to robust convergence of GMRES+AMG.

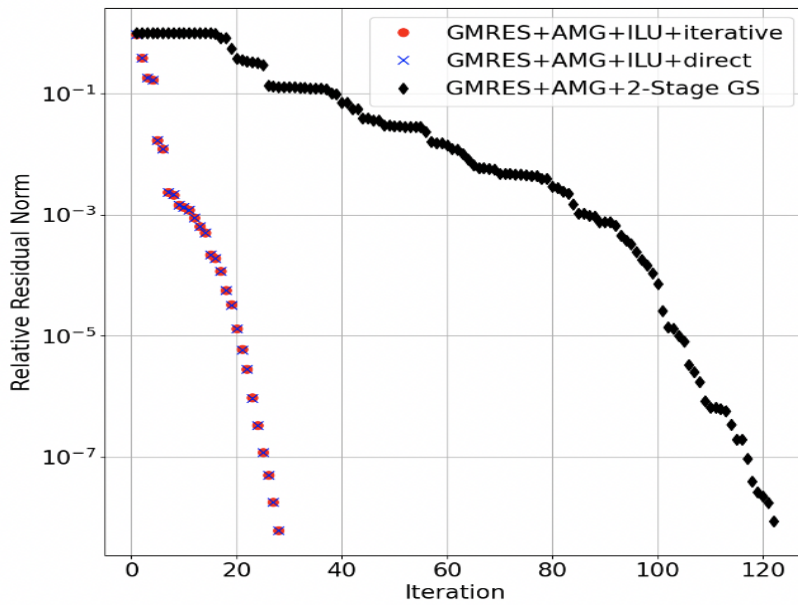


FIGURE 9 Convergence histories of (F)GMRES+AMG with polynomial Gauss-Seidel and ILU(0) smoothers using direct and iterative solves. $N = 11M$

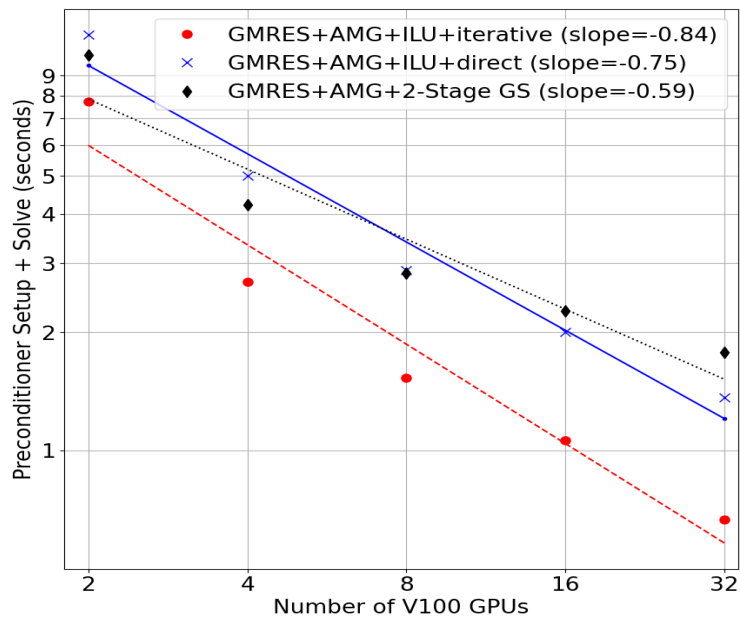


FIGURE 10 Strong-scaling of (F)GMRES+AMG with ILU(0) smoothers using direct and iterative solves. hypre-BoomerAMG GPU results on NREL Eagle. Matrix size $N = 11M$.

In order to further improve the efficiency of the PeleLM (F)GMRES+AMG pressure solver on many-core GPU architectures, AMG V -cycles with ILU smoothing on the finest levels are combined with a polynomial smoother on the remaining coarse levels. It was found that the convergence rates for mixed AMG are almost identical to using ILU on all levels, thus leading to significant cost reductions. For a large problem $N = 11M$ solved on the NREL Eagle supercomputer the iterative solve for LDU with row scaling led to a 5X speed-up over the direct solve within the GMRES+AMG V -cycles. Furthermore, the strong scaling curve for the solver run time is close to linear.

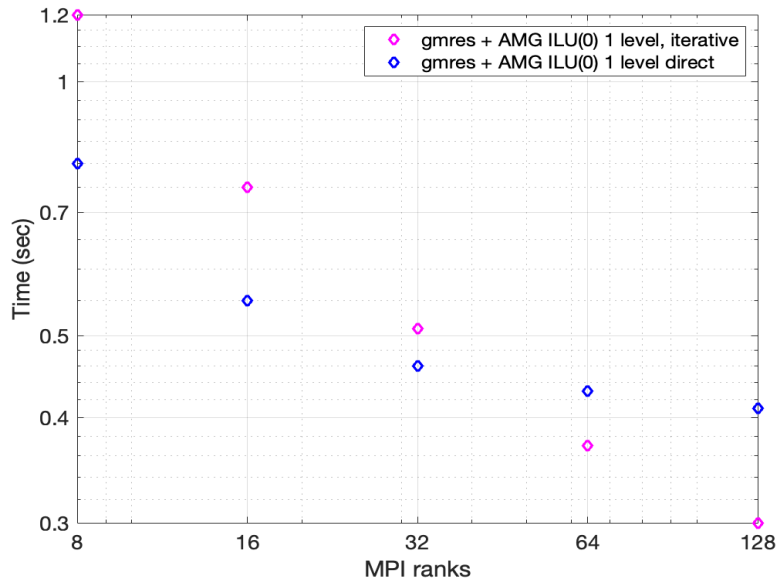


FIGURE 11 hypre-BoomerAMG GPU results on ORNL Crusher with AND MI250X. PeleLM model. $N = 11M$

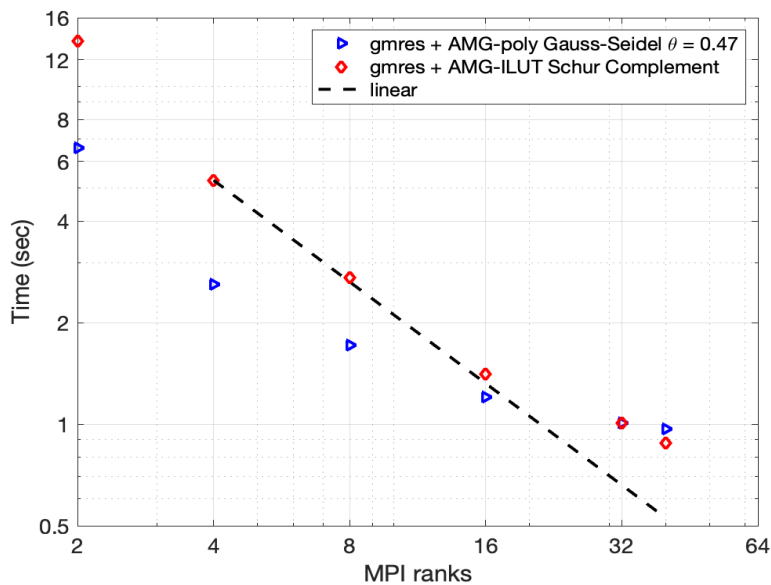


FIGURE 12 Nalu-Wind NREL 5MW wind turbine mesh. Strong-scaling of (F)GMRES+AMG with ILUT Schur Complement using iterative solves versus polynomial Gauss-Seidel smoother. Matrix size $N = 23M$

For the Nalu-Wind pressure continuity equation, an ILUT Schur complement smoother with iterative solves on the local block diagonal systems was applied. Pressure linear systems from NREL 5 MegaWatt reference turbine simulations were employed to assess numerical accuracy and performance. The linear solver exhibits improved parallel strong-scaling characteristics with this new smoother and maintains a constant GMRES iteration count when the number of GPU compute nodes increases. By omitting the residual computations from the single iteration of the GMRES-Schur solver, to overall execution time is reduced. Our future plans include implementing the fixed-point iteration algorithms of Chow³⁸ to compute the ILU factorization on GPUs. The Schwarz preconditioners described in Prenter³⁹ and Jomo et al.³⁷ could also be adapted to hypre for PeleLM. The solver has also

been incorporated into the MFIX-Exa CFD-DEM model⁴⁰ for carbon capture and chemically reacting fluid flows. The solver leads to at least 5X improvement in the computational speed on GPUs.

ACKNOWLEDGMENTS

This work was authored in part by the National Renewable Energy Laboratory, operated by Alliance for Sustainable Energy, LLC, for the U.S. Department of Energy (DOE) under Contract No. DE-AC36-08GO28308. Funding was provided by the Exascale Computing Project (17-SC-20-SC), a collaborative effort of two U.S. Department of Energy organizations (ASCR and the NNSA). The data that support the findings of this study are available from the corresponding author upon reasonable request. We thank the anonymous reviewers for their suggestions, which led to several valuable improvements.

References

1. Saad Y. *Iterative Methods for Sparse Linear Systems*, 2nd Ed. SIAM; 2003.
2. Nonaka A, Bell JB, and Day MS. A conservative, thermodynamically consistent numerical approach for low Mach number combustion. I. Single-level integration. *Combust Theor Model*. 2018;**22**(1):156–184.
3. Thomas SJ, Ananthan S, Yellapantula S, Hu JJ, Lawson M, and Sprague MA. A Comparison of Classical and Aggregation-Based Algebraic Multigrid Preconditioners for High-Fidelity Simulation of Wind Turbine Incompressible Flows. *SIAM Journal on Scientific Computing*. 2019;**41**(5):S196–S219.
4. Fischer P, Kerkemeier S, Min M, Lan YH, Phillips M, Rathnayake T, et al. NekRS, a GPU-accelerated spectral element Navier–Stokes solver. *Parallel Computing*. 2022;**114**:102982.
5. Argonne National Laboratory. Nek5000; 2023. <https://nek5000.mcs.anl.gov/>.
6. Arndt D, Fehn N, Kanschat G, Kormann K, Kronbichler M, Munch P, et al. ExaDG: High-order discontinuous Galerkin for the exa-scale. In: *Software for exascale computing-SPPEXA 2016-2019*. Springer International Publishing; 2020. p. 189–224.
7. Anzt H, Chow E, and Dongarra J. Iterative sparse triangular solves for preconditioning. In: *European conference on parallel processing*. Springer; 2015. p. 650–661.
8. Chow E, Anzt H, Scott J, and Dongarra J. Using Jacobi iterations and blocking for solving sparse triangular systems in incomplete factorization preconditioning. *Journal of Parallel and Distributed Computing*. 2018;**119**:219–230.
9. Chow E, and Saad Y. Experimental study of ILU preconditioners for indefinite matrices. *Journal of Computational and Applied Mathematics*. 1997;**86**:387–414.
10. Van der Sluis A. Condition numbers and equilibration of matrices. *Numerische Mathematik*. 1969;**14**(1):14–23.
11. Bauer FL. Optimally scaled matrices. *Numerische Mathematik*. 1963;**5**(1):73–87.
12. Stewart GW. *Matrix Algorithms: Volume 1: Basic Decompositions*. SIAM; 1998.
13. Henrici P. Bounds for iterates, inverses, spectral variation and fields of values of non-normal matrices. *Numerische Mathematik*. 1962;**4**(1):24–40.
14. Falgout RD, Jones JE, and Yang UM. The Design and Implementation of hypre, a Library of Parallel High Performance Preconditioners. In: Bruaset AM, and Tveito A, editors. *Numerical Solution of Partial Differential Equations on Parallel Computers*. Berlin, Heidelberg: Springer Berlin Heidelberg; 2006. p. 267–294.
15. Chow E, and Vassilevski PS. Multilevel block factorizations in generalized hierarchical bases. *Numerical Linear Algebra with Applications*. 2003;**10**(1-2):105–127.

16. Mallowney P, Li R, Thomas S, Ananthan S, Sharma A, Rood J, et al. Preparing an Incompressible-Flow Fluid Dynamics Code for Exascale-Class Wind Energy Simulations. In: Proceedings of Supercomputing 2021. IEEE/ACM; 2021. p. 1–12.
17. Ern A, and Giovangigli V. Fast and Accurate Multicomponent Transport Property Evaluation. J Comput Phys. 1995;**120**:105–116.
18. Kee RJ, Ruply RM, Meeks E, and Miller JA. 1996. *CHEMKIN-III: A FORTRAN Chemical Kinetics Package for the Analysis of Gas-phase Chemical and Plasma Kinetics*. SAND96-8216. Livermore: Sandia National Laboratories.
19. Zhang W, and et al. AMReX: A Framework for Block-Structured Adaptive Mesh Refinement. Journal of Open Source Software. 2019;**4**(37):1370.
20. Falgout RD, and Meier-Yang U. hypre: A Library of High Performance Preconditioners. In: International Conference on computational science; 2002. p. 632–641.
21. Ruge JW, and Stüben K. Algebraic multigrid. In: Multigrid methods. SIAM; 1987. p. 73–130.
22. Xu T, Li R, and Osei-Kuffuor D. A two-level GPU-accelerated incomplete LU preconditioner for general sparse linear systems. Numer Linear Algebra Appl. 2020;Submitted for publication.
23. Falgout RD, Li R, Sjögreen B, Wang L, and Yang UM. Porting hypre to heterogeneous computer architectures: Strategies and experiences. Parallel Computing. 2021;**108**:102840. Available from: <https://www.sciencedirect.com/science/article/pii/S0167819121000867>.
24. Li R, and Zhang C. Efficient Parallel Implementations of Sparse Triangular Solves for GPU Architecture. In: Proceedings of SIAM Conference on Parallel Proc. for Sci. Comput.; 2020. p. 118–128.
25. Ipsen IC. 1998. *A note on the field of values of non-normal matrices*. . North Carolina State University. Center for Research in Scientific Computation.
26. Elsner L, and Paardekooper M. On measures of nonnormality of matrices. Linear Algebra and its Applications. 1987;**92**:107–123.
27. Eiermann M. Fields of values and iterative methods. Linear Algebra and its Applications. 1993;**180**:167–197. Available from: <https://www.sciencedirect.com/science/article/pii/0024379593905302>.
28. Thomas S, Carr A, Mallowney P, Li R, Świrydowicz K, and Day M. Neumann Series in GMRES and Algebraic Multigrid Smoothers. arXiv preprint arXiv:211214681. 2022;.
29. Verbeek M, Cullum J, and Joubert W. 2002. *AMGToolBox*. . Los Alamos National Laboratory.
30. Carr A, de Sturler E, and Gugercin S. Preconditioning Parametrized Linear Systems. SIAM Journal on Scientific Computing. 2021;**43**(3):A2242–A2267.
31. Davis TA, and Hu Y. The University of Florida sparse matrix collection. ACM Transactions on Mathematical Software (TOMS). 2011;**38**(1):1–25.
32. Saad Y, and Schultz MH. GMRES: A generalized minimal residual algorithm for solving nonsymmetric linear systems. SIAM Journal on scientific and statistical computing. 1986;**7**(3):856–869.
33. Baker AH, Falgout RD, Kolev TV, and Yang UM. Multigrid Smoothers for Ultraparallel Computing. SIAM J Sci Comput. 2011;**33**:2864–2887.
34. Li R, Sjögreen B, and Meier-Yang U. A new class of AMG interpolation operators based on matrix matrix multiplications. To appear SIAM Journal on Scientific Computing. 2020;.
35. Joubert W, and Cullum J. Scalable Algebraic Multigrid on 3500 processors. Electronic Transactions on Numerical Analysis. 2006;**23**:105–128.

36. Yang UM. On long range interpolation operators for aggressive coarsening. *Numerical Linear Algebra with Applications*. 2010;**17**:453–472.
37. Jomo J, Oztoprak O, de Prenter F, Zander N, Kollmannsberger S, and Rank E. Hierarchical multigrid approaches for the finite cell method on uniform and multi-level hp-refined grids. *Computer Methods in Applied Mechanics and Engineering*. 2021;**386**:114075.
38. Chow E, and Patel A. Fine-Grained Parallel Incomplete LU Factorization. *SIAM Journal on Scientific Computing*. 2015;**37**(2):C169–C193.
39. de Prenter F, Verhoosel CV, van Brummelen EH, Evans JA, Messe C, Benzaken J, et al. Multigrid solvers for immersed finite element methods and immersed isogeometric analysis. *Computational Mechanics*. 2020;**65**:807–838.
40. Musser J, Almgren AS, Fullmer WD, Antepara O, Bell JB, Blaschke J, et al. MFIX-Exa: A path toward exascale CFD-DEM simulations. *The International Journal of High Performance Computing Applications*. 2022;**36**(1):40–58.

How to cite this article: Thomas S. J., Carr, A. K., Mallowney, P. Świrydowicz K., and Day, M. (2022), Scaled ILU Smoothers for Navier-Stokes Pressure Projection, *NAME*, *VOL*.